Available online at www.sciencedirect.com
SCIENCE DIRECT®

Journal of the European Ceramic Society 23 (2003) 2633–2637
www.elsevier.com/locate/jeurceramsoc

High frequency dielectric properties of $Ba(Mg_{1/3}Ta_{2/3})O_3$ complex perovskite ceramics

I-Nan Lin[a,*], Chih-Ta Chia[c], Hsiang-Lin Liu[c], Yi-Chun Chen[c], Hsiu-Fung Cheng[c], Cheng-Chung Chi[b]

[a]*Materials Science Center, National Tsing Hua University, Hsinchu, 300 Taiwan, ROC*
[b]*Department of Physics, National Tsing Hua University, Hsinchu, 300 Taiwan, ROC*
[c]*Department of Physics, National Taiwan Normal University, Taipei, 117, Taiwan, ROC*

Abstract

The dielectric properties of $Ba(Mg_{1/3}Ta_{2/3})O_3$ and $Ba(Mg_{1/3}Nb_{2/3})O_3$ ceramics were investigated using Fourier transformed infrared and Raman spectroscopies. The real part of dielectric constant of these materials decreases when the heavier Ta atoms replaced the lighter Nb atoms, which is closely related to the shift of mode-frequency. The *Q*-factor of the materials depends weakly on the composition. The decrease in *Q*-factor with the frequency is due to the presence of a resonance mode at around 3 THz. Larger width of the breathing Raman mode, A_{1g}[O], correlates very well with the lower *Q*-value of the BMN materials, as compared with the BMT materials.

Keywords: Ba(Mg,Ta,)O_3 materials; FTIR spectroscopy; Microwave ceramics; Dielectric properties; Raman spectroscopy

1. Introduction

Complex perovskites with general formula $A(B_{1/3}B'_{2/3})O_3$, where $A = Ba^{2+}$, $B = Mg^{2+}$, Zn^{2+} or Ni^{2+}, $B' = Ta^{5+}$ or Nb^{5+} show very interesting properties at microwave frequencies, such as high permittivity ε', low dielectric loss ε'' and small temperature coefficient of resonance frequency.[1–5] Therefore, these materials are commonly used as resonators in microwave devices. High *Q*-factor is of the most concern. Generally, the dielectric losses in microwave dielectrics, which reduce the *Q*-factor could be induced either intrinsically or extrinsically. The intrinsic losses are related to material composition and crystal structure, which are less process dependent, whereas the extrinsic losses are related to defects (vacancies, impurities), structural disorder, porosity or second phases...etc, which are more process dependent. The studies on dielectric properties of the materials are sometimes controversial, which is primarily due to the interference of extrinsic dielectric loss on the measured dielectric characteristics. The most promising approach to understand the intrinsic microwave dielectric properties of the materials is to study their higher frequency response, including the submillimeter and infrared regime, since the intrinsic losses are overwhelmingly stronger than the extrinsic ones[6–9] in the far-infrared regime. Some dielectric ceramics have been investigated in submillimeter and infrared waves range by using backward-wave-oscillator (BWO), FTIR spectroscopy[10,11] and coherent terahertz (THz) time domain spectroscopy.[12–14] Moreover, the investigation of order–disorder structure by Raman method is a subject of considerable interest[15,16] recently.

In microwave regime, $Ba(Mg_{1/3}Nb_{2/3})O_3$ (BMN) materials exhibit much larger power loss and hence lower *Q*-factor than $Ba(Mg_{1/3}Ta_{2/3})O_3$ (BMT) materials. Therefore, these materials were chosen in this paper for investigation in submillimeter by using THz time domain, Fourier transformed infrared (FTIR) and Raman spectroscopy, in an attempt to understand the correlation between materials' characteristics and their complex dielectric constant.

2. Experimental

$Ba(Mg_{1/3}Ta_{2/3})O_3$ and $Ba(Mg_{1/3}Nb_{2/3})O_3$ ceramic samples, which are abbreviated as BMN and BMT, respectively, were prepared by conventional mixed

* Corresponding author.
E-mail address: inlin@mx.nthu.edu.tw (I-N. Lin).

0955-2219/03/$ - see front matter © 2003 Elsevier Ltd. All rights reserved.
doi:10.1016/S0955-2219(03)00160-2

oxide process, in conjunction with a hot isostatic pressing (HIP) technique. These samples were first conventionally sintered at 1580 °C in air and then hot isostatic pressed in 99.9% Ar atmosphere using a Mo chamber.

In the FTIR measurements, near-normal infrared reflectance spectra were taken at room temperature on mechanically polished surfaces of high density polycrystalline samples. A Bruker IFS 66v Fourier transform infrared spectrometer was used in the far-infrared and mid-infrared regions (40–4000 cm^{-1}). The modulated light beam from the spectrometer was focused onto either the sample or an Au reference mirror, and the reflected beam was directed onto a 4.2 K bolometer detector (40–600 cm^{-1}) and a B-doped Si photoconductor (450–4000 cm^{-1}). The different sources, beam splitters, and detectors used in these studies provided substantial spectral overlap, and the reflectance mismatch between adjacent spectral ranges was less than 1%. The optical properties i.e., the complex conductivity $\sigma(\omega)=\sigma_1(\omega) + I\sigma_2(\omega)$ or dielectric function $\varepsilon(\omega)=1 + 4\pi i\sigma(\omega)/\omega$, were calculated from Kramers-Kronig analysis of the reflectance data.[15] To perform these transformations one needs to extrapolate the reflectance at both low and high frequencies. At low frequencies the extension was done by modeling the reflectance using the Lorentz model and using the fitted results to extend the reflectance below the lowest frequency measured in the experiment. The high-frequency extrapolations were done by using a weak power law dependence, $R\sim\omega^{-s}$ with $s\sim1$–2.

Meanwhile, a DILOR XY 800 triple-grating Raman spectrometer equipped with a liquid-nitrogen-cooled CCD was used for micro-Raman measurements. The 514.5nm line of an Ar^+ ion laser with output 10 mW was used as the excitation source and Olympus BH-2 microscope with 100× objective was employed for room temperature micro-Raman detection. The recorded Raman spectra exhibited approximately 1 cm^{-1} resolution.

In THz measurements, the THz transient produced by illuminating the GaAs-photoconducting antenna with ultrashort laser pulses was directed onto the BMT (BMN) samples, serving as pump pulse. The scattered THz transient is collected and reflected by an off-axis paraboloidal mirror and then is focused onto the electro-optic crystal. A second optical pulse (probe pulse), delayed with respect to the pump pulse by a variable amount, probes the change in the index of refraction by passing through the crystal. The change of the probe-pulse polarization yields information on both the amplitude and phase of the THz field. The details of the setup for THz transmission measurements have been described elsewhere.[13,14] In this THz experiment, reference data is first obtained without the sample between the transmitter and the receiver. Subsequently, a sample was introduced in the path of the THz beam and a second set of data is taken. The spectra of THz transient can be obtained by applying a fast Fourier transform (FFT) to the time domain waveform. Dividing the spectra obtained with a sample by the spectra obtained without a sample yields the transmission function $t(\omega)$ of the sample

$$t(\omega)=\left(\frac{4N_s}{(N_s+1)^2}\right)\exp(i(k_s-k_v)d), \quad (1)$$

where $N_s=n+ik$ is the complex index of refraction of sample, $k_s=\omega N_s/c$ & $k_i=\omega/c$, ω is the frequency, d is the thickness of the sample and c is the speed of light in vacuum. Eq. (1) can be solved numerically.

3. Results and discussion

Fig. 1 shows the room-temperature infrared reflectance of the BMT and BMN samples, indicating that a number of phonon features are observed in the far-infrared frequency regime. The FTIR spectra of the two materials are very similar with each other. The real part of the dielectric function, ε_{IR}', and the imaginary part of the dielectric function, ε_{IR}'', can be derived from the Kramers-Kronig analysis of the reflectance curves. As the FTIR measurements were performed at $f>1.2$ THz (40 cm^{-1}) frequency regime, which is about three orders of magnitude higher than the frequency regime for microwave dielectric properties measurements (∼several GHz). How accurate do the FTIR-derived microwave dielectric properties represent the dielectric behavior of the materials in microwave regime is not clear. Terahertz spectroscopy in 0.1–0.6 THz regimes was thus performed to fill the dielectric properties in this frequency gap.

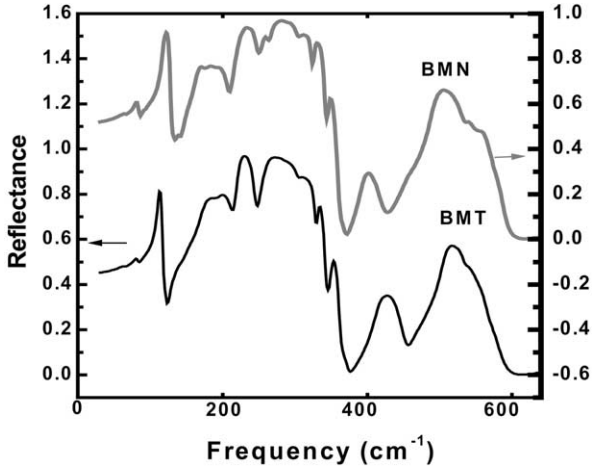

Fig. 1. Room-temperature infrared reflectance spectra for the $Ba(Mg_{1/3}Ta_{2/3})O_3$ and $Ba(Mg_{1/3}Nb_{2/3})O_3$ materials.

The results of terahertz (THz) spectroscopic measurements for BMT and BMN materials, the real part of dielectric constant, ε_{THz}', and the quality factor, $Q_{THz}=\varepsilon_{THz}'/\varepsilon_{THz}''$, are shown in Fig. 2(a) and (b), respectively. These figures indicate that, in 0.1–0.6 THz regime, the ε_{THz}' of these materials hardly changes, whereas the Q-factor decreases monotonously, with increasing frequency. Moreover, the ε_{THz}'-value for BMT materials is markedly smaller than that for BMN materials and the Q-value for BMT materials is pronouncedly higher than that for BMN materials. To facilitate the comparison, the frequency response of the ε'- and Q-values derived from FTIR spectroscopy were also plotted in Fig. 3a and b, respectively, for the frequency regime upto 180 cm^{-1} (5 THz), the first resonance peak. These figures indicate that FTIR spectroscopy derived dielectric properties, when extrapolated toward low frequency regime, fit very well with the dielectric parameters measured by terahertz spectroscopy, that is, the FTIR-derived dielectric parameters represent quite well the dielectric behavior for these materials.

These results imply that FTIR measurement down to 1.2 THz (40 cm^{-1}) is necessary and sufficient in order to accurately describe the microwave dielectric behavior of the BMT and BMN materials, since there exists no resonance peak below 1.2 THz (40 cm^{-1}). FTIR measurement up to 800 cm^{-1} frequency regime is enough to include all the possible resonance phenomenon, as the dielectric constant (ε'-value) derived from FTIR at 800 cm^{-1} ($\varepsilon'=3.0$–2.0) is about the same as the dielectric constant measured by optical spectroscopy (not shown).

To model the dielectric behavior of the materials using Lorentz algorithm[15] for understanding the true mechanism resulting in the compositional dependence of the dielectric properties, it is necessary to accurately assign a vibrational mode for each of the resonance peaks in FTIR spectra. Unfortunately, the FTIR resonance peaks are usually very broad, overlapping each other (Fig. 1). It is practically impossible to unambiguously assign the vibrational mode for the resonance peaks in FTIR spectra. In contrast, resonance peaks in Raman spectra are usually very sharp, which can more clearly illustrate the effect of atomic substitution on the vibrational characteristics of the materials.

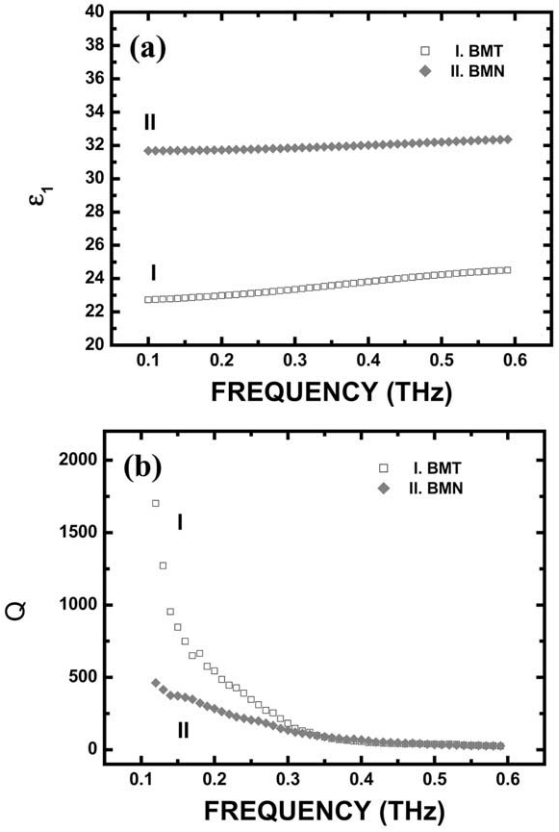

Fig. 2. The frequency dependence of (a) the real part of dielectric constant, ε', and (b) the quality factor of the dielectric function, $Q=\varepsilon'/\varepsilon''$, for $Ba(Mg_{1/3}Ta_{2/3})O_3$ and $Ba(Mg_{1/3}Nb_{2/3})O_3$ materials derived from Terahertz spectroscopy in 0.1–0.6 THz.

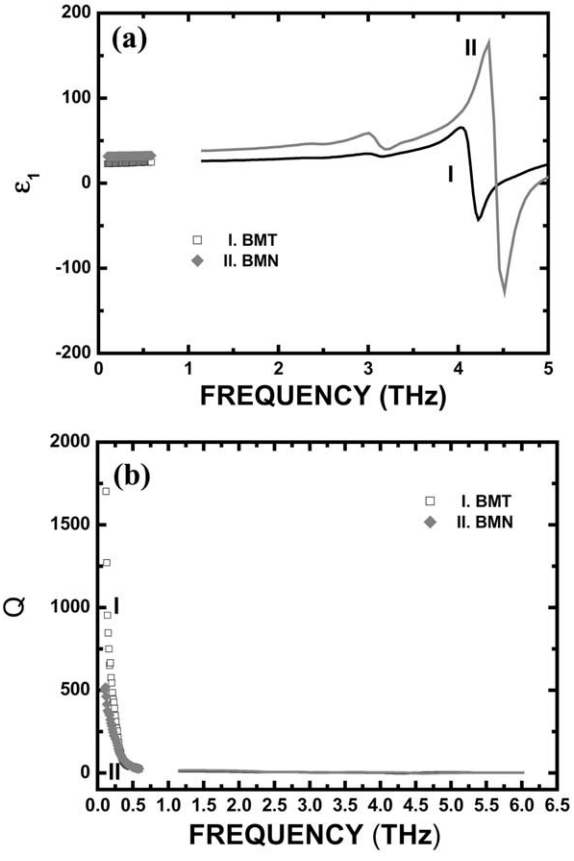

Fig. 3. The frequency dependence of (a) the real part of dielectric constant, ε', and (b) the quality factor of the dielectric function, $Q=\varepsilon'/\varepsilon''$, for $Ba(Mg_{1/3}Ta_{2/3})O_3$ and $Ba(Mg_{1/3}Nb_{2/3})O_3$ materials in 0.01–5 THz regime (discreet symbols are those derived from Terahertz spectroscopy and continuous curves are those derived from FTIR spectroscopy).

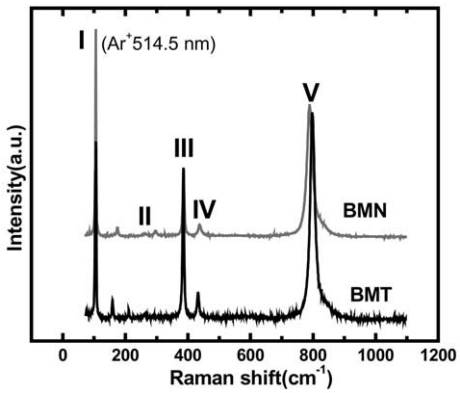

Fig. 4. (a) Raman spectra of $Ba(Mg_{1/3}Ta_{2/3})O_3$ and $Ba(Mg_{1/3}Nb_{2/3})O_3$ materials measured at room temperature. The assignment for the Raman peaks are: I. $A_{1g}[Ba]+E_g[Ba]$ mode, II. $A_{1g}(Ta,Nb)+E_g(Ta,Nb)$ mode, III. $A_{1g}[Ba+O]+E_g[Ba+O]$ mode, IV. $E_g[O]$ mode and V. $A_{1g}[O]$ mode.

Fig. 4 depicts the Raman spectra of BMT and BMN materials at room temperature. All the Raman peaks are of narrow line width, which is intimately correlated with highly ordered structure and high-Q characteristics of the materials. Four dominated peaks are found, they are peaks near 105, 386, 437 and 788 cm^{-1}. Similar Raman spectra have been reported in the literatures,[17–19] and the phonon modes have recently been unambiguously assigned.[20] The highest mode ($\sim$788 cm^{-1}) is the breathing vibration of oxygen octahedron, i.e. $A_{1g}[O]$ (mode V). The peak near 437 cm^{-1} is $E_g[O]$ (mode IV), which shift slightly with composition. The modes insensitive to composition are $A_{1g}[Ba]+E_g[Ba]$ modes around 105 cm^{-1} (mode I) and $A_{1g}[Ba+O]+E_g[Ba+O]$ around 386 cm^{-1} (mode III). Moreover, the three weak signals at 150–300 cm^{-1}, which are heavily dependent on the composition, are assigned as $A_{1g}(Ta,Nb)+E_g(Ta,Nb)$ (mode II).

Table 1 shows the relative Raman shift of the phonon modes with the composition. Most peaks show red shift behavior, i.e., shift to lower frequency as the heavier Ta-atoms replaced the lighter Nb-atoms. The mode II phonons, which exhibit most marked red shift when the lager ionic sized Ta is present, are designated as the vibrational mode correlated with the resonant vibration of Ta^{5+}–Ta^{5+} (or Nb^{5+}–Nb^{5+}) layers. This mode contributes insignificantly to the dielectric properties to the materials, as they are non-dipole phonons. The mode V phonon around 788 cm^{-1}, the Ta^{5+}–O^{2-} (or Nb^{5+}–O^{2-}) breathing mode ($A_{1g}[O]$), is the only blue-shifted Raman peak. The blue shifting is ascribed to the stiffer Ta–O bonds, as compared with the Nb–O bonds. The $A_{1g}(O)$ phonon has the largest width and an asymmetric tail at higher frequency, as indicated in Fig. 4. The small high-frequency tail of $A_{1g}(O)$ phonon found in Fig. 4 is presumed due to the mutual exchange of Mg with Ta or Nb positions in unit cell, and this also causes the disorder in trigonal sample structure.

The breathing mode is a dipole phonon and hence contributes large proportion of dielectric behavior for the materials. The full width at half maximum (FWHM) of $A_{1g}(O)$ phonon is markedly larger for BMN materials, as compared with that for BMT materials, indicating that the $(NbO_6)^{n-}$ oxygen octahedral cage is less tightly bonded than the $(TaO_6)^{n-}$ oxygen octahedral cage.[18] These results imply that narrower Raman peaks, especially the breathing mode of $(TaO_6)^{n-}$ (or $(NbO_6)^{n-}$) octahedrons, are intimately correlated with the higher Q-factor for the materials.

Raman phonons and IR phonons are complementary to each other. The IR phonons are very difficult to model, while the Raman phonons can be more clearly defined. Understanding on the behavior of Raman phonons provides some information about how the external factors such as frequency and compositions influence the dielectric properties of the materials, especially when there is vibrational modes, which are both Raman and IR active. In BMT (BMN) materials, Raman phonons are totally complementary to IR phonons and hence will have no contribution to the dielectric properties of the materials. However, the factors shifting and broadening the Raman resonance peaks are expected to have similar influence on the IR resonance peaks. Therefore, understanding the characteristics of Raman phonons can still provide some insight to the behavior of IR phonons.

Table 1
The variation of the characteristics of Raman modes with the materials composition[a]

	Raman Peak	BMN (cm^{-1})	BMT (cm^{-1})	Remark
I.	$A_{1g}[Ba]+E_g[Ba]$	105	105	Invariant
II.	$A_{1g}(Ta,Nb)+E_g(Ta,Nb)$	180–300	155–260	Red shift[b]
III.	$A_{1g}[Ba+O]+E_g[Ba+O]$	386	386	In variant
IV.	$E_g[O]$	437	433	Red shift[b]
V.	$A_{1g}[O]$	788 ($\Delta f=20.2$)	796.4 ($\Delta f=17.0$)	Blue shift[b]

[a] The assignment of Raman modes follows Ref. 20.

[b] The red shift indicates that the resonance peak shifts toward lower frequency, whereas the blue shift means that the resonance peak shifts in reversed direction, when the heavier Ta atoms replaced the lighter Nb atoms.

4. Conclusions

In order to study the effect of the niobium substitution for tantalum in barium magnesium tantalate (BMT) complex perovskite materials, the dielectric properties of $Ba(Mg_{1/3}Ta_{2/3})O_3$ and $Ba(Mg_{1/3}Nb_{2/3})O_3$ ceramics were investigated using and pulsed terahertz (THz) time domain spectroscopy from 0.1 to 0.6 THz, Fourier transformed infrared spectroscopy from 40 to 800 cm^{-1} and Raman spectroscopy. The complex dielectric constant of such materials was obtained in both of the above frequency ranges. The Q-factor of the materials depends weakly on composition. The increase of loss is due to some resonance modes above 1.2 THz.

References

1. Nomura, S., Toyama, K. and Kaneta, K., *Jpn. J. Appl. Phys.*, 1982, **21**, L642.
2. Onada, M., Kuwata, J., Kaneta, K., Toyama, K. and Nomura, S., *Jpn. J. Appl. Phys*, 1982, **21**, 1707.
3. Nomura, S., *Ferroelectrics*, 1983, **49**, 61.
4. Nomura, S., Konoike, T., Sakabe, Y. and Wakino, K., *J. Am. Ceram. Soc.*, 1984, **67**, 59.
5. Guo, R., Shalla, A. S. and Cross, L. E., *J. Appl. Phys*, 1994, **75**, 4704.
6. Petzelt, J. *et al.*, *Ferroelectrics*, 1989, **93**, 77.
7. Rupprecht, G. O. and Bell, R. O., *Phys. Rev.*, 1962, **125**, 1915.
8. Silverman, B. D., *Phys. Rev.*, 1962, **125**, 1921.
9. Gurevich, V. L. and Tagantsev, A. K., *Adv. Phys*, 1991, **40**, 719.
10. Petzelt, J., Zurmuhlen, R., Bell, A., Kamba, S., Kozlov, G. V., Volkov, A. A. and Setter, N., *Ferroelectrics*, 1992, **133**, 205.
11. Petzelt, J., Kamba, S., Kozlov, G. V. and Volkov, A. A., *Ferroelectrics*, 1996, **176**, 145.
12. Kuzel, P. and Petzelt, J., *Ferroelectrics*, 2000, **239**, 949.
13. Tsai, T. R., Liang, M. H., Hu, C. T., Chi, C. C. and Lin, I. N., *Jpn J. Appl. Phys*, 2000, **39**, 5642.
14. Tsai, T. R., Liang, M. H., Hu, C. T., Chi, C. C. and Lin, I. N., *J. Eur. Ceram. Soc.*, 2001, **21**, 2787.
15. Moreira, R. L., Matinaga, F. M. and Dias, A., *Appl. Phys. Lett.*, 2001, **78**, 428.
16. Galasso, F. S., *Structure, Properties and Preparation of Perovskite-Type Compounds*,, 1st ed.. Pergamon, Oxford, 1969.
17. Siny, I. G., Tao, R. W., Katiyar, R. S., Guo, R. A. and Bhalla, A. S., *J. Phys. Chem. Solids*, 1998, **59**, 181.
18. Siny, I. G., Katiyar, R. S. and Bhalla, A. S., *J. Raman Spectro*, 1998, **29**, 385.
19. Tamura, H., Sagala, D. A. and Wakino, K., *Jpn. J. Appl. Phys., Part 1*, 1986, **25**, 787.
20. Chia, C. T., Cheng, H. S., Liu, H. L. and Lin, I. N., *J. Appl. Phys.* (in press).